A new magnetic bearing using Halbach magnet arrays for a magnetic levitation stage

Young-Man Choi (최영만),[1,a)] Moon G. Lee (이문구),[2] Dae-Gab Gweon (권대갑),[1] and Jaehwa Jeong (정재화)[3,b)]
[1]*Department of Mechanical Engineering, Korea Advanced Institute of Science and Technology (KAIST), 373-1 Kusung-Dong, Yusong-Gu, Daejon 305-701, Republic of Korea*
[2]*Division of Mechanical Engineering, Ajou University, San 5, Wonchon-Dong, Yeongtong-Gu, Suwon-City, Gyeonggi-Do 443-749, Republic of Korea*
[3]*Department of Control and Instrumentation Engineering, Korea University, 208 Seochang-Ri, Jochiwon-Eup, Youngi-Gun, Chungnam 339-700, Republic of Korea*

(Received 19 August 2008; accepted 19 March 2009; published online 20 April 2009)

Next-generation lithography requires a high precision stage, which is compatible with a high vacuum condition. A magnetic levitation stage with six degrees-of-freedom is considered state-of-the-art technology for a high vacuum condition. The noncontact characteristic of magnetic levitation enables high precision positioning as well as no particle generation. To position the stage against gravity, z-directional electromagnetic levitation mechanisms are widely used. However, if electromagnetic actuators for levitation are used, heat is inevitably generated, which deforms the structures and degrades accuracy of the stage. Thus, a gravity compensator is required. In this paper, we propose a new magnetic bearing using Halbach magnet arrays for a magnetic levitation stage. The novel Halbach magnetic bearing exerts a force four times larger than a conventional magnetic bearing with the same volume. We also discuss the complementary characteristics of the two magnetic bearings. By modifying the height of the center magnet in a Halbach magnetic bearing, a performance compromise between levitating force density and force uniformity is obtained. The Halbach linear active magnetic bearing can be a good solution for magnetic levitation stages because of its large and uniform levitation force. © *2009 American Institute of Physics.*
[DOI: 10.1063/1.3116482]

I. INTRODUCTION

Magnetic levitation (maglev) technology is one of the solutions for a high-precision positioning mechanism in a high vacuum environment because of its noncontact nature. It does not need any fluid supply or exhaust, which would lower the degree of vacuum. With no mechanical connection, mechanical stress in a fixed frame is not transferred to the moving platform on which a specimen is laid. Also, frictionless movement gives excellent scanning performance. Magnetic levitation can be achieved by implementing six degree-of-freedom (DOF) motion, with all DOFs actively controlled by multiple actuators and sensors. Thus, active vibration isolation and/or high static stiffness can be achieved by servo-control.[1] Conventional positioning stages have relatively low structural natural frequencies, which limit control bandwidth due to complex structural and mechanical connections. However, the maglev stage can achieve high bandwidth because it has a single moving body without mechanical connections.

In the late 1980s, a first concept for a magnetically levitated positioning technique was developed by Trumper *et al.*[2] Many mechanisms have been refined from his technique, or newly developed technique.[1,3,4] Figure 1 represents the schematic of a dual-servo positioning system, which has a maglev fine stage. For long range movement, the coarse stage moves with long strokes, and the fine stage is positioned with high accuracy and small strokes. Upon the coarse stage, the fine stage is levitated by several one DOF actuators. The one DOF z-direction actuator between the fine stage and the coarse stage is called a linear active magnetic bearing (LAMB). Three or more LAMBs levitate the fine stage and control its out-of-plane motion. The LAMB uses electromagnetic force to control its vertical motion. However, if only electromagnetic force by electric current is used, continuous power consumption is inevitable to suspend the weight of the moving platform. In this case, the heat generated by coil current deforms the mechanical structure and deteriorates system accuracy. Thus, we need a gravity compensating mechanism. In order to compensate for gravity, mechanical springs, air-bellows, and opposed permanent magnets[5–9] have been discussed. Among these, springs and air-bellows are inevitably mechanically coupled, which limits the control bandwidth of the fine stage. The opposed permanent magnets have no mechanical contact and high force, but show nonlinear force characteristics. Hol *et al.*[10] proposed a new gravity compensator using permanent magnets and a Lorentz coil. Two vertically magnetized stator magnet rings suspend two horizontally magnetized mover magnet rings inside. Due

a)Present address: National Institute of Standards and Technology, Gaithersburg, Maryland.
b)Author to whom correspondence should be addressed. Electronic mail: jaehwa@korea.ac.kr. Tel.: +82-41-860-1765. FAX: +82-41-865-1820.

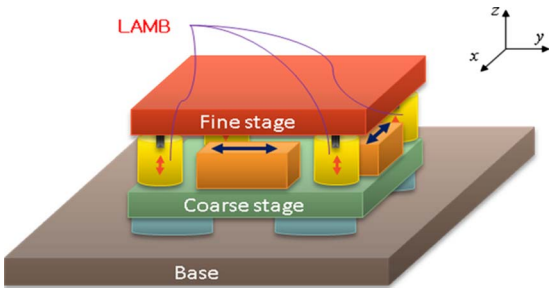

FIG. 1. (Color online) Dual servo system using six DOF magnetically levitated fine stage. The fine stage is levitated by several one-DOF actuators. The LAMB is the one-DOF z-direction actuator between the fine stage and the coarse stage.

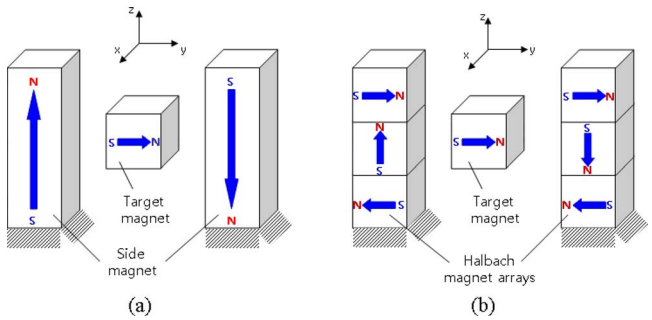

FIG. 2. (Color online) Conceptual models: (a) conventional gravity compensator and (b) proposed gravity compensator. The side magnets of the proposed gravity compensator include not only vertically magnetized magnets but also horizontally magnetized magnets.

to the uniform magnetic field made by the long stator magnets, the mover magnets have constant levitation force. Also, a circular Lorentz coil between the two mover magnet rings generates a position-independent force to control the position of the mover. A LAMB such as this gravity compensator is very useful for a high-precision maglev stage using dual-servo configuration. It can control out-of-plane motion by actively compensating the gravity of the stage simultaneously.

As stated earlier, the biggest advantage of the maglev stage is high bandwidth, which works to reduce settling times and improve disturbance rejection. For its higher bandwidth, the gravity compensator, as well as other embodied actuators, should have high force density, which is given as generated force per volume of permanent magnets used. Moreover, the gravity compensator should have a uniform and constant levitating force and a small parasitic force, even though the position has deviated from the nominal position. Force variation is directly related to bearing stiffness. If the force variation were large, internal modes due to bearing stiffness deteriorate dynamic performance when feedback control is applied. Although most magnetic bearings are said to have zero stiffness, the stiffness is zero only at their nominal positions, and it changes significantly around the nominal position. Therefore, it is important to have near-zero stiffness within the whole workspace.

In this paper, we propose a new active magnetic bearing for a magnetic levitation stage using Halbach magnet arrays[11] and Lorentz coils. Because the Halbach magnet array can confine magnetic flux density, the proposed magnetic bearing exerts more levitation force than the conventional one. Also, the Lorentz coil can make the dynamic force to control its vertical motion with the confined magnetic field using Halbach magnet arrays. This active magnetic bearing is called a Halbach LAMB (HLAMB). Due to its large force capacity and embodied Lorentz coils, the HLAMB has a compact size. Moreover, the HLAMB is designed to have near-zero stiffness within its workspace.

This paper is organized as follows. In Sec. II, the configuration of HLAMB is introduced. The new gravity compensating mechanism is compared with a conventional one using three-dimensional finite element analysis (3D FEA) in order to prove its superior performance. In Sec. III, an analytical electromagnetic model for HLAMB is established. In Sec. IV, we discuss the force characteristics of both gravity compensating mechanisms and investigate a compromising parameter between two mechanisms. In Sec. V, a design optimization is applied to the HLAMB. A prototype is fabricated and tested. Conclusions are presented in Sec. VI.

II. CONCEPT OF THE HALBACH LINEAR ACTIVE MAGNETIC BEARING

A. Design considerations

In order to achieve high-precision positioning ability and good dynamic performance, the bearing should be designed properly. A LAMB for a six-DOF maglev fine stage should have following characteristics:

A. Gravity compensation with no power consumption.
B. Large force density.
C. Zero stiffness.
D. Position-independent dynamic force.
E. Enough workspace in all directions.

As mentioned previously, the LAMB should compensate for gravity as exactly as possible to avoid heat problems. The large force density can reduce the volume and mass of the bearing; thus, force density is related to the efficiency of the LAMB. Zero stiffness is important for vibration isolation and servo-stability. Also, zero stiffness means that force nonlinearity is negligible and no additional skill like a feedback linearization is required. In order to reduce control complexity, the dynamic force should be position-independent and be linear with respect to driving current. Finally, for six-DOF motion, the LAMB should have adequate working volume without any contact.

B. Conceptual design

In this section, we introduce the basic configuration of a new magnetic bearing. First, we simplify the structure of the gravity compensator from former research[10] as shown in Fig. 2(a). The side magnets are longer than the target magnet and they are magnetized vertically. The horizontally magnetized target magnet is levitated in the z-direction by two side magnets. The upper poles of the side magnets attract the target magnet, and the lower poles repulse it. In this case, the levitating force is uniform even when the target magnet deviates from the nominal position. This is because the magnetic field around the target magnet is uniform due to relatively long

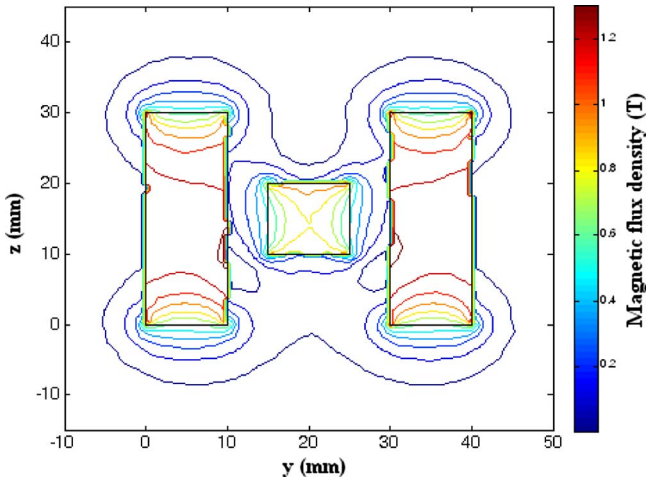

FIG. 3. (Color online) Contour plot of magnetic flux density of conventional gravity compensator. This figure represents the magnetic field in the *YZ* cross section at the geometric center of the conventional gravity compensator.

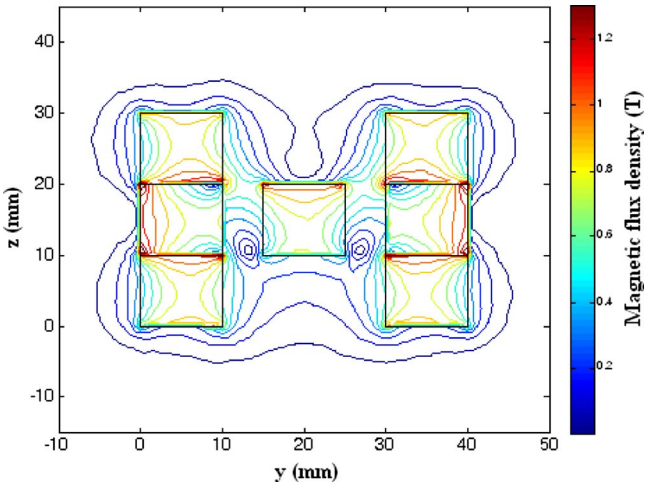

FIG. 4. (Color online) Contour plot of magnetic flux density of proposed gravity compensator. This figure represents the magnetic field in the *YZ* cross section at the geometric center of the proposed gravity compensator.

side magnets. The magnetic characteristics are analyzed using 3D FEA. The size of the side magnet is $10\times10\times30$ mm^3, and the size of the target magnet is $10\times10\times10$ mm^3. The gap between the side magnet and the target magnet is 5 mm. For simplicity, we did not consider the *x*-directional effect since it can be diminished by increasing the thickness of the side magnet. Figure 3 represents the magnetic field in the *YZ* cross section at the geometric center of the conventional gravity compensator. As previously mentioned, the field around the target magnet is uniform. However, it results in only a small force for levitation—FEA results show that the force in the *z*-direction is only 5.7 N.

Therefore, we propose a new gravity compensating mechanism. To enlarge the force density, we need to focus magnetic flux to both poles of the target magnet. A Halbach magnetic array confines the magnetic flux to one side of the magnet array, which has an orthogonally magnetized magnet.[11] Inspired by Halbach's conception, we divided the side magnet into three magnets as shown in Fig. 2(b). They push up the target magnet more strongly than the conventional gravity compensator because the distance between the *N* pole and *S* pole becomes smaller. Figure 4 shows the magnetic field of a new gravity compensator with the same volume as a conventional one. The magnetic field is focused to both poles of the target magnet. In this case, the *z*-directional force is 23.4 N. It has a force four times larger than by the conventional one. Moreover, due to the focused magnetic flux, a Lorentz coil can be contained compactly in the proposed mechanism. For high dynamic force, the Lorentz coil should be located at the point where the magnetic field density is high. As shown in Fig. 4, the magnetic field in the middle of both Halbach magnet arrays is not strong enough. Near the Halbach magnet array the magnetic field is strong, but the direction is not exactly horizontal. However, if two coils are located symmetrically, the resultant force has only a component in the *z*-direction, and the resultant moment becomes zero. If the magnetic field around the coils is uniform, the dynamic force depends only on current, and the relation between them becomes linear. Due to the Halbach magnet array, the proposed LAMB can have a uniform magnetic field near the horizontally magnetized segments. The schematic for the proposed LAMB is shown in Fig. 5. The two Lorentz coils and the target magnet are fixed together on the ground (actually, on a coarse stage) as a stator and the two Halbach magnet arrays are fixed on the moving platform (actually, on a fine stage) as a mover. The new magnetic bearing is a HLAMB.

III. MODELING

In order to model the magnetic field generated by permanent magnets, we obtained an analytical model for a simple block magnet using a surface current model.[12] The total magnetic field can then be obtained by superposition of the magnetic field for each block magnet. Finally, the force induced to the target magnet can be calculated.

A. Analytical model for a permanent magnet block

Figure 6 shows a surface current model for a block magnet. Assuming that the magnetization is in the *z*-direction, the surface current flows by the right hand rule as shown in Fig. 6. The equivalent current density J is given as $\mu_0 M$, where

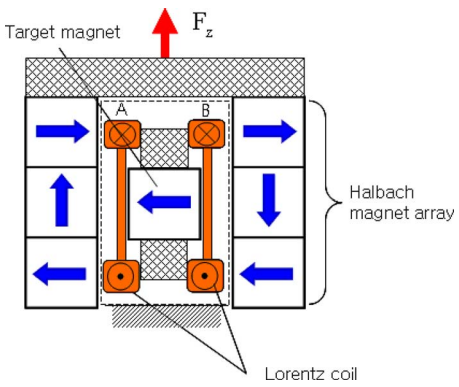

FIG. 5. (Color online) Concept of HLAMB. The two Lorentz coils and the target magnet are fixed together on the coarse stage as a stator and the two Halbach magnet arrays are fixed on the fine stage as a mover.

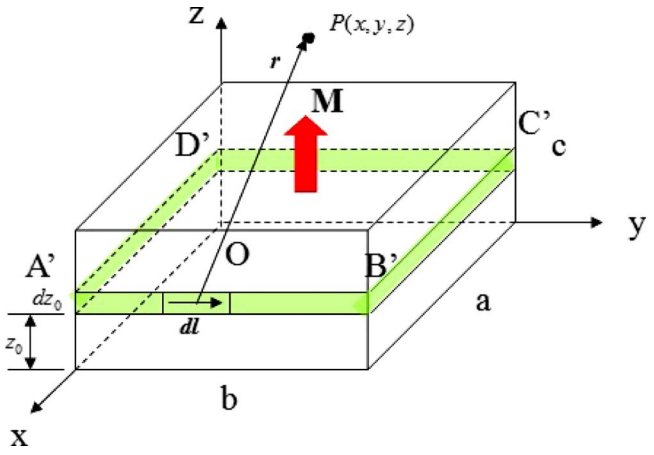

FIG. 6. (Color online) Surface current model of a block magnet. Assuming that the magnetization is in the z-direction, the surface current flows by the right hand rule as shown.

M is the magnetization of the permanent magnet. Considering a rectangular sheet A'B'C'D' with infinitesimal thickness dz, the magnetic field at $\boldsymbol{P}$ by the sheet can be obtained by Biot–Savart's law, given as

$$d\boldsymbol{B}=\frac{\mu_0}{4\pi}\frac{Id\boldsymbol{l}\times\boldsymbol{r}}{r^2}, \tag{1}$$

where $\mu_0=4\pi\times10^{-7}$ is the magnetic permeability of air, I is the current through the sheet coil, $\boldsymbol{r}$ is a vector from a current unit, $d\boldsymbol{l}$ is to the filed point $\boldsymbol{P}$. Integrating the result along the contour A'B'C'D' and z-axis, the total magnetic field at any point, $\boldsymbol{P}(x,y,z)$ out of the magnet can be calculated,

$$\begin{aligned}\boldsymbol{B}_M(x,y,z)&=B_x\boldsymbol{i}+B_y\boldsymbol{j}+B_z\boldsymbol{k}\\&=\int_0^c(dB_x(z_0)\boldsymbol{i}+dB_y(z_0)\boldsymbol{j}+dB_z(z_0)\boldsymbol{k}),\end{aligned} \tag{2}$$

where dB_x, dB_y, and dB_z are the magnetic induction components in the x, y, and z directions, respectively, at $\boldsymbol{P}(x,y,z)$ produced by the current loop A'B'C'D'.

B. Calculation of the static and dynamic force

The static force $\boldsymbol{F}_S$ and moment $\boldsymbol{M}_S$ applied to the target magnet are given as Eqs. (3) and (4). The electromagnetic body force is an integral of the inner product of the Maxwell stress tensor $\boldsymbol{T}$ and the surface normal $\boldsymbol{n}$ over the surface of the target magnet,[13]

$$\boldsymbol{F}_s=\int\boldsymbol{T}\times\boldsymbol{n}da=\int\nabla\times\boldsymbol{T}dv \tag{3}$$

$$\boldsymbol{M}_s=\int\boldsymbol{r}\times(\boldsymbol{T}\boldsymbol{n})da, \tag{4}$$

where da and dv are the infinitesimal surface area and volume of the target magnet, respectively.

The Maxwell stress tensor is

$$\begin{aligned}T&=\frac{1}{\mu_0}\left(\boldsymbol{B}\boldsymbol{B}-\frac{1}{2}B^2\delta\right)\\&=\frac{1}{\mu_0}\begin{bmatrix}B_x^2-\frac{1}{2}B^2 & B_xB_y & B_xB_z\\ B_xB_y & B_y^2-\frac{1}{2}B^2 & B_yB_z\\ B_xB_z & B_yB_z & B_z^2-\frac{1}{2}B^2\end{bmatrix},\end{aligned} \tag{5}$$

where $\boldsymbol{B}$ is the total magnetic field whose components are $[B_x\ B_y\ B_z]$, B is the magnitude of $\mathbf{B}$, and $\boldsymbol{\delta}$ is the identity tensor.

The dynamic force can be also calculated by Eq. (3). However, doing so is computationally expensive because all magnetic flux components by the coil current should be calculated. Therefore, we used the Lorentz law under the assumption that the magnetic flux produced by the coils does not affect the static force of the target magnet. The effective volume of the coil, whose length is the same as the width of the Halbach magnet array, is considered to obtain the Lorentz force. Then, the dynamic force $\boldsymbol{F}_D$ and moment $\boldsymbol{M}_D$ of the HLAMB are given as

$$\boldsymbol{F}_D=-\int\int\int_V\boldsymbol{J}\times\boldsymbol{B}_Mdv=-\int\int_A\left(\frac{I}{A}\int_0^l d\boldsymbol{y}\times\boldsymbol{B}_M\right)dA \tag{6}$$

$$\begin{aligned}\boldsymbol{M}_D&=-\int\int\int_V(\boldsymbol{r}-\boldsymbol{p})\times\boldsymbol{J}\times\boldsymbol{B}_Mdv\\&=-\int\int_A\left(\frac{I}{A}\int_0^l(\boldsymbol{r}-\boldsymbol{p})\times d\boldsymbol{y}\times\boldsymbol{B}_M\right)dA,\end{aligned} \tag{7}$$

where A is the cross-sectional area of the coil, I is the current flowing in the coil, l is effective length of the coil, and vector $(\boldsymbol{r}\text{-}\boldsymbol{p})$ is defined as the position of the infinitesimal volume dv from the center of gravity of the whole permanent magnet system.

IV. PERFORMANCE OF THE HALBACH LINEAR ACTIVE MAGNETIC BEARING

Using the preceding analytical model, we calculate the force distribution with regard to variations of the height (z-direction) and the gap (y-direction) from the nominal position. Since the maximum stroke of the fine maglev stage is set to ±1 mm in the y-z plane, we obtained force distribution within this workspace. It should be noted that the z-directional stroke is actually much smaller than 1 mm.

Figure 7 shows the force distribution of the conventional magnetic bearing. From Fig. 7(a), the nominal levitating force is around 5.7 N. The levitating force is almost insensitive to the variation of gap, whereas it increases with the height variation. At two ends of the z stroke, maximum z-directional stiffness equals 100 N/m. The parasitic force in

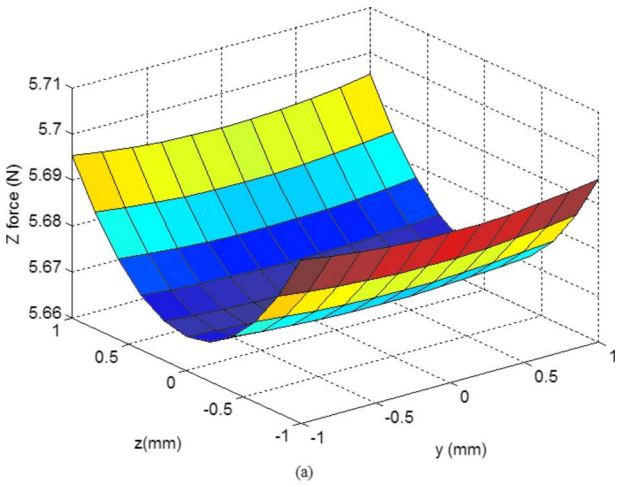

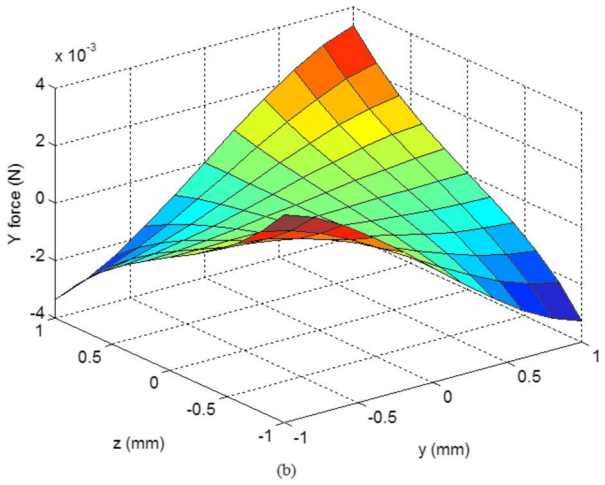

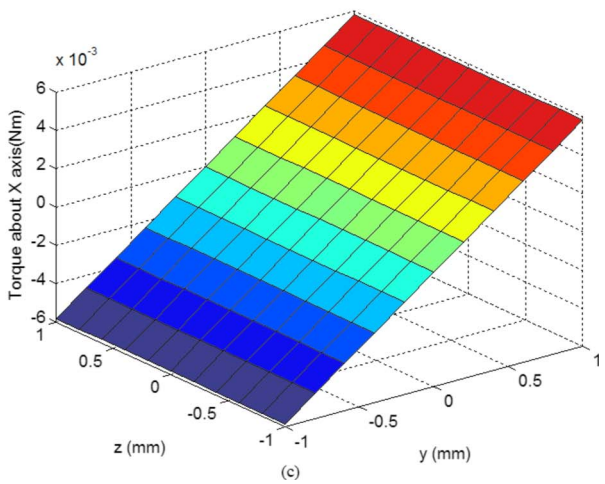

FIG. 7. (Color online) Static force distribution of the conventional gravity compensator, (a) *Z* force, (b) *Y* force, and (c) torque about *X* axis. The levitating force is almost insensitive to the variation of gap, but the nominal levitating force is just around 5.7 N.

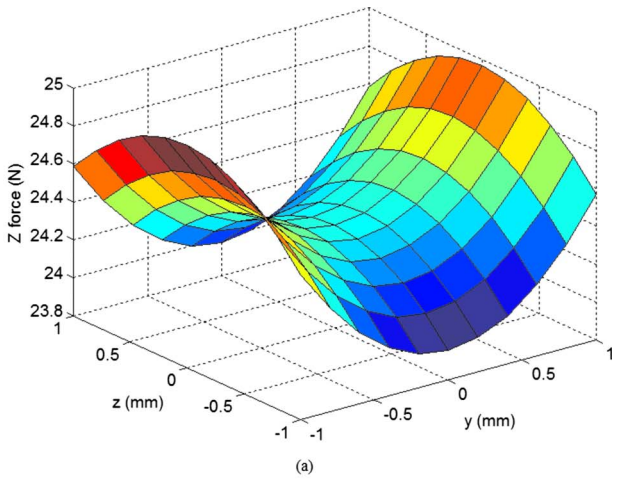

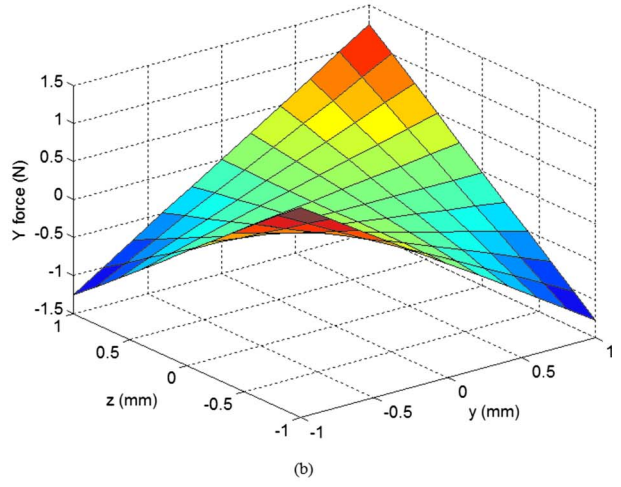

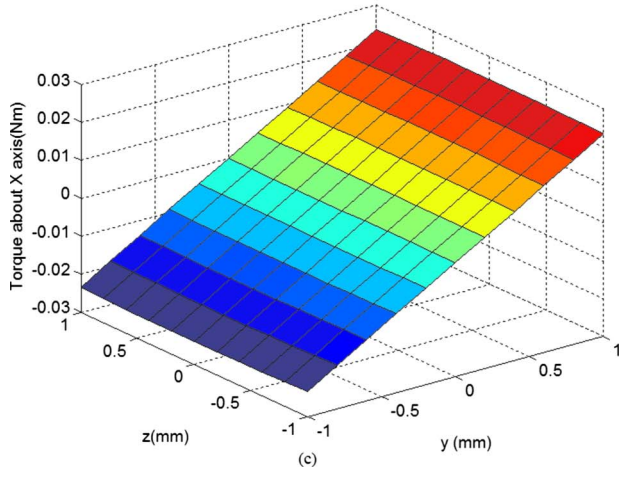

FIG. 8. (Color online) Static force distribution of the Halbach linear active magnetic bearing, (a) *Z* force, (b) *Y* force, and (c) torque about *X* axis. The nominal levitating force is 24.3 N, which is more than four times the force of the conventional system. The distribution is similar to the shape of a saddle.

y-direction and the torque about *x*-axis are negligibly small, as shown in Figs. 7(b) and 7(c).

For the Halbach magnetic bearing, the levitating force is greatly increased as shown in Fig. 8(a). Matching the previously described 3D FEA result, the nominal levitating force is 24.3 N, which is more than four times the force of the conventional system. The distribution is similar to the shape of a saddle. Contrary to the conventional gravity compensator, the sign of *z*-direction stiffness becomes reversed. The maximum stiffness in the *z*-direction is 1440 N/m. The maximum parasitic force in the *y*-direction is about 1.2 N at the corners of the workspace, as shown in Fig. 8(b). For reference, the static stiffness of a variable-reluctance actuator is

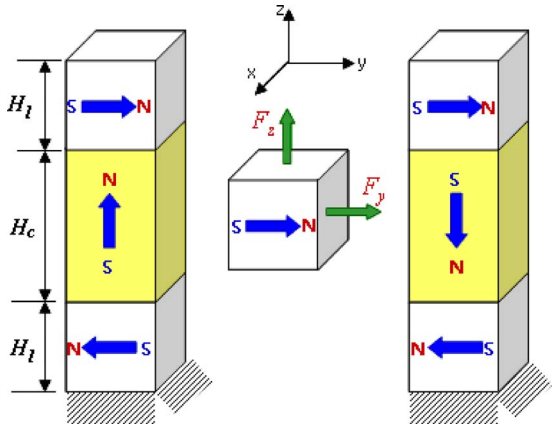

FIG. 9. (Color online) Modification of Halbach magnet array in the HLAMB. H_c is the height of the center magnet and H_l is the height of the upper and the lower magnets.

on the order of 10^4-10^5 N/m. Although a Halbach magnetic bearing has much less static stiffness than a variable-reluctance actuator, it is necessary to lower the stiffness for the highest possible performance.

The conventional gravity compensator can achieve uniform and constant force due to the relatively long vertical magnets compared to the target magnet. This inspires us to find a compromise solution through geometric variation with the previous conceptual Halbach magnetic bearing. In the Halbach magnet array, the upper and lower magnets work on confining the magnetic field to the target magnet, while the center magnet acts as a path for magnetic flux. If the height of the center magnet in the Halbach magnet array were extended as presented in Fig. 9, the confining effect would be weakened, but the magnetic field around the target magnet would become more uniform. Figure 10 shows the effect of increasing the Halbach ratio—the height of the center magnet to the height of the lower magnet. Even though the levitating force is reduced as the height is increased, the parasitic force in the *y*-direction and the *z*-directional stiffness force is also diminished. Also, there exists a toggle point where the absolute value of the *z*-direction stiffness becomes nearly zero. This is because the magnetic field around the target magnet is uniform at this point.

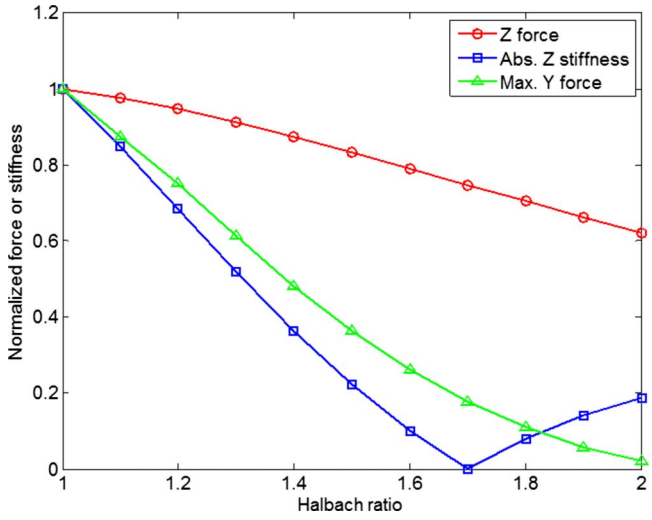

FIG. 10. (Color online) Force characteristics of HLAMB vs Halbach ratio. The Halbach ratio is the ratio of the height of the center magnet to the height of the lower magnet. Even though the levitating force is reduced as the Halbach ratio is increased, the parasitic force in the *y*-direction and the variation of the levitating force is also diminished. There exists a toggle point where the absolute value of the *z*-direction stiffness becomes nearly zero.

TABLE I. Optimization results and final design parameters.

	Design parameters	Unit
Halbach ratio	2.2	
Width of Halbach magnets	40	mm
Thickness of Halbach magnets	7.8	mm
Gap	7.2	mm
Height of lower magnet	10	mm
Thickness of target magnet	10	mm
Width of lower magnet	10	mm
Height of target magnet	10	mm
Total size	$40\times40\times42$	mm^3
Static *Z* force	24.45	N
Dynamic *Z* force	6.53	N
Max. *Z* stiffness	11.2	N/m
Max. *Y* force	0.024	N
Max. Torque about *x*-axis	0.025	Nm
Power @ cont. 20 N dynamic force	28.2	W
Natural freq. of internal mode	0.34	Hz

V. DESIGN OPTIMIZATION

To fulfill the design considerations discussed in Sec. II, design optimization is required. In this case, it might be the minimization of the cost function, $f(x)$ that is dependent on the design parameters. The cost function might be subject to constraints. In the design of the HLAMB, we wish to maximize dynamic force when the following constraints are satisfied:

- *Z -direction static force* should be equal to the gravity of the moving platform. Because the mass of the moving platform is 10 kg, four HLAMBs should generate a static force of $2.5\ \text{kg}\times9.8\ \text{m/s}^2=24.5$ N.
- *Maximum z-direction static stiffness* should be lower than 1 N/m, which makes the natural frequency of the static bearing less than 0.1 Hz. Because the servo-bandwidth will be about 100 Hz, the effect of the static stiffness can be considered negligible.
- *Maximum parasitic force in the y-direction* direction should be lower than 0.05 N because the thrust force of 100 N and the servo-bandwidth of 100 Hz can reject this parasitic force.
- Its *size* should be limited for implementation and assembly. The maximum volume of the HLAMB is restricted to $40\times40\times50\ \text{mm}^3$.

The optimization design process is realized using sequential quadratic programming.[14] At each major iteration, a positive-definite quasi-Newton approximation of the Hessian of the Lagrangian function is calculated using the Broden–Fletcher–Goldfarb–Shanno method. This method generally guarantees the local minimum.[15] However, we need a best solution in the design boundary. Using a Bayesian stopping

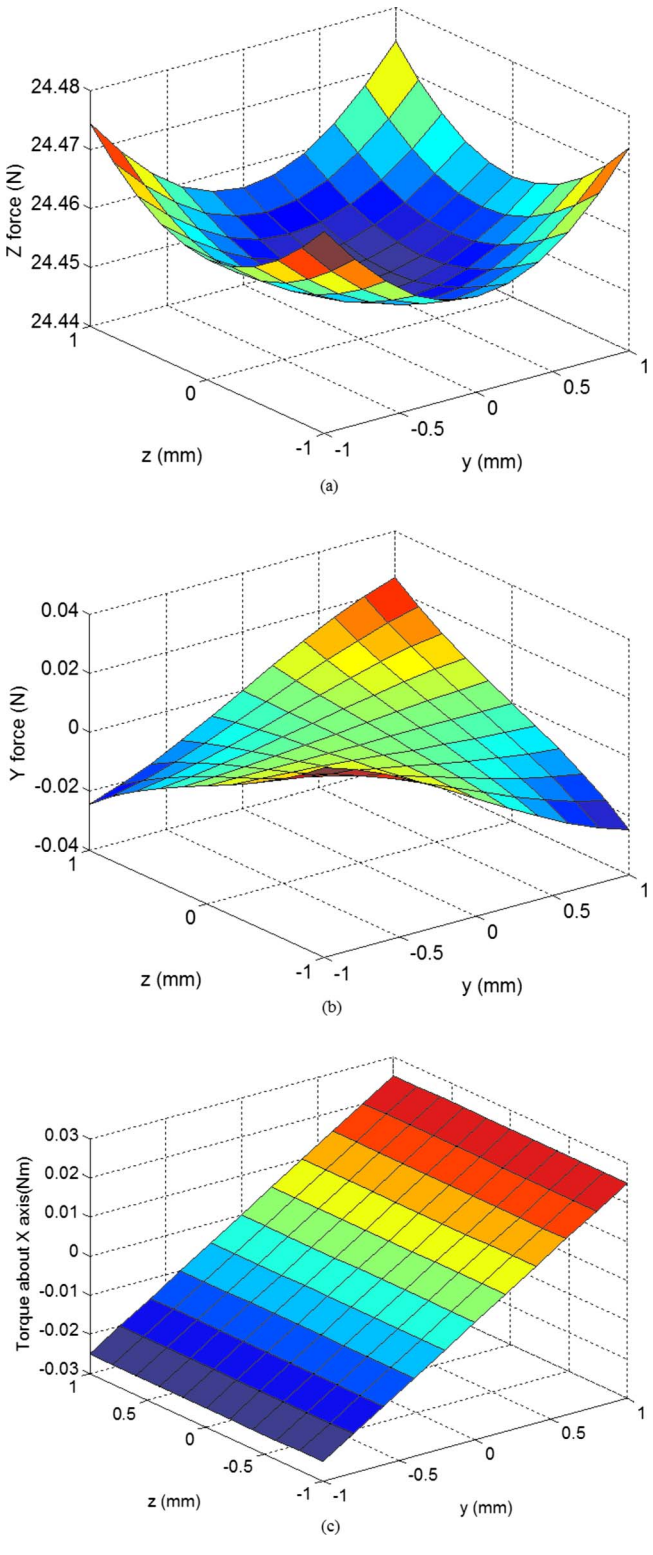

FIG. 11. (Color online) Static force distribution of the final HLAMB design: (a) *Z* force, (b) *Y* force, and (c) torque about *X* axis.

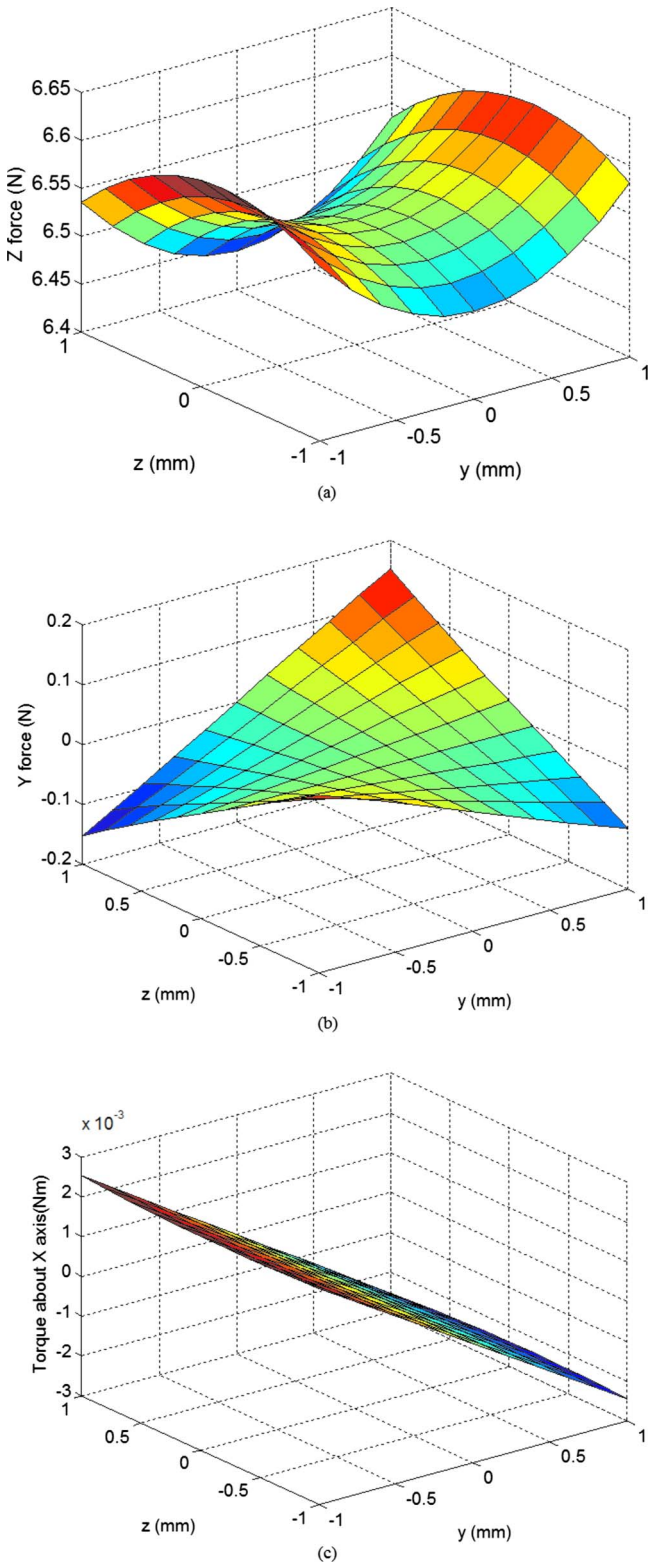

FIG. 12. (Color online) Dynamic force distribution of the final HLAMB design: (a) *Z* force, (b) *Y* force, and (c) torque about *X* axis.

rule,[16] a global minimum can be found statistically with random initial estimations of design parameters. The whole optimization process is performed using the MATLAB optimization toolbox. The cost function and the constraints are updated at every iteration by the analytical model of the HLAMB obtained as described in Sec. III. The analytical model is also implemented by MATLAB code. Other parameters and magnetic properties are fixed for simplicity. The target magnet's size is set to $10\times10\times10$ mm^3. All permanent magnets are NdFeB45-*M* grade magnets (Stargroup Industry Co. Ltd., Daegu, Republic of Korea). This grade has a remanent magnet flux (Br) of 1.35 T and intrinsic coercive force (iHc) of 1195 kA/m. The air gap between the Halbach

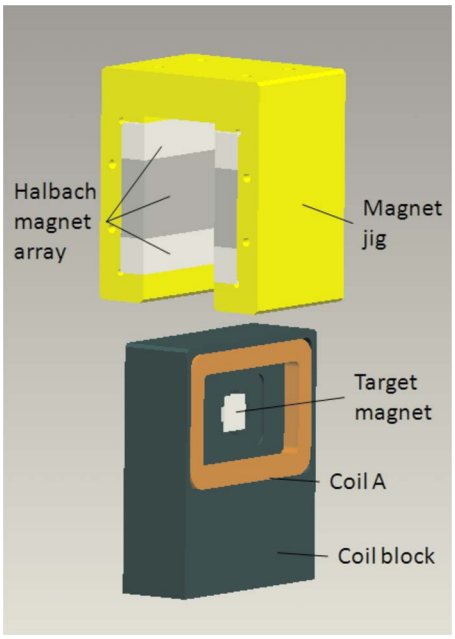

FIG. 13. (Color online) Exploded view of HLAMB prototype. Halbach magnet arrays, which are assembled in the magnet jig, are a mover and the coil block is a stator.

magnets and coil is set to 1.5 mm to obtain a 1 mm stroke and some margin. Each coil winding has 108 turns with a copper core whose diameter is 0.5 mm, and an insulating layer whose thickness is 0.025 mm. The results from design optimization are shown in Table I. The static force distribution and dynamic force distribution of the final HLAMB design are shown in Figs. 11 and 12, respectively.

From the results of the design optimization, the geometric parameters of the prototype of the HLAMB are decided. Figure 13 shows the designed prototype. Halbach magnet arrays are assembled in the magnet jig, which should be a "mover." The magnet jig is made of aluminum alloy (6061-T6). Two coil windings and one target magnet are assembled in a monolithic coil block. To eliminate eddy currents, the coil block is made of black acryl, and the coils and target magnet are fixed to the coil block by adhesive without screws. This coil block is a "stator." The total size is about $40 \times 55 \times 65$ mm^3.

To evaluate the force characteristics of the prototype, a three-axis load cell (MAS121, CAS®) was used. Figure 14 shows the test setup. The load cell can measure the forces in the z-direction and y-direction, and the moment about the x-axis. The position of the mover can be changed by the three-axis manual stage. The forces at one position are measured for 5 s with 5 kS/s. Then, the time-averaged forces are recorded at 11×11 positions in the YZ workspace. First, the static forces are depicted in Fig. 15. The nominal Z force is about 23.6 N, which is only a 3.5% difference from the design. The variations in the parasitic forces are quite small. However, the actual force distribution has some differences from the design. As compared to Fig. 11(a), the Z force distribution has an inclination. Also, the Y force has an offset. These phenomena are caused by assembling error of the Halbach magnet array. The Halbach magnet array is hard to assemble because of its very large escaping force. Thus, a

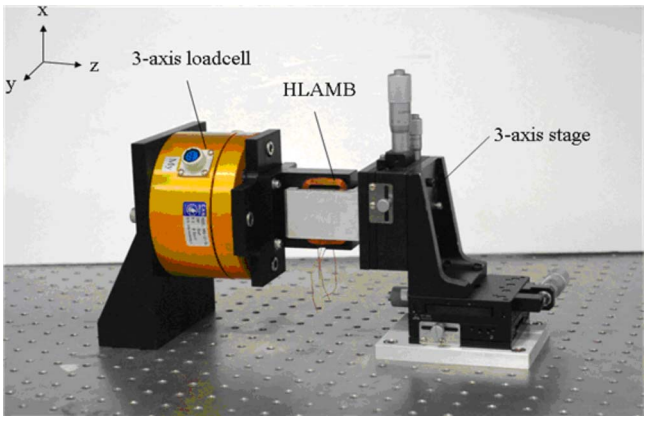

FIG. 14. (Color online) Test setup for HLAMB prototype. To evaluate the force characteristics of the prototype, a three-axis load cell was used.

relatively large assembly error occurred in the fabrication process even though an assembly jig and strong epoxy with short curing time were used. In this prototype, the upper left magnet juts about 0.3 mm beyond the inside plane of the Halbach magnet array. This asymmetry caused the inclination and the offset of the force distributions. These offset

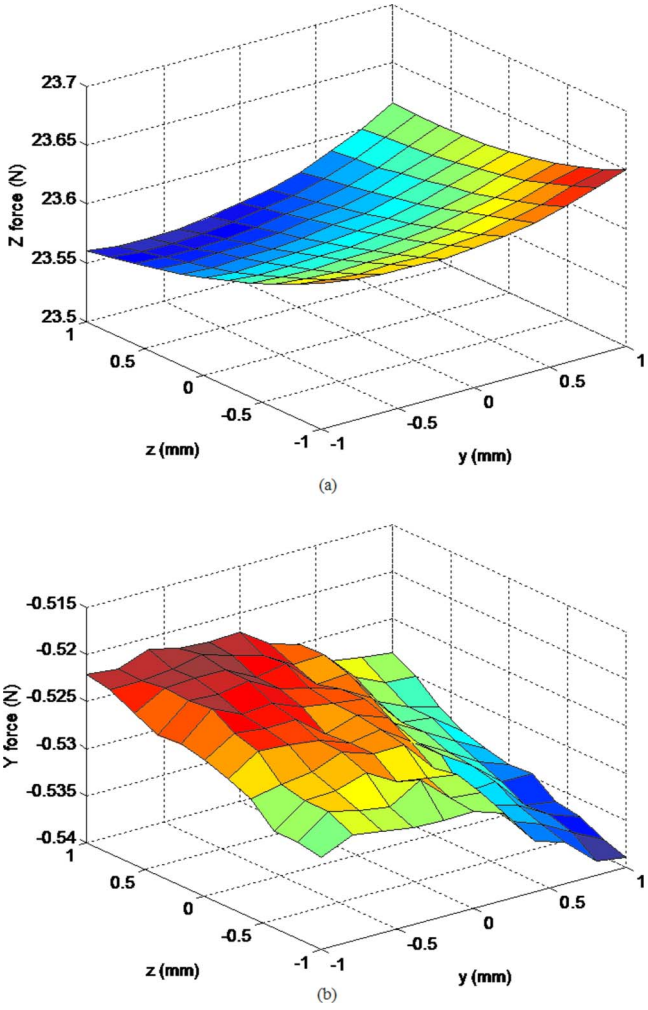

FIG. 15. (Color online) Static force distribution of the prototype: (a) Z force, and (b) Y force. The measured nominal Z force is about 23.6 N, which is only a 3.5% difference from the design. The variations of the parasitic forces are quite small.

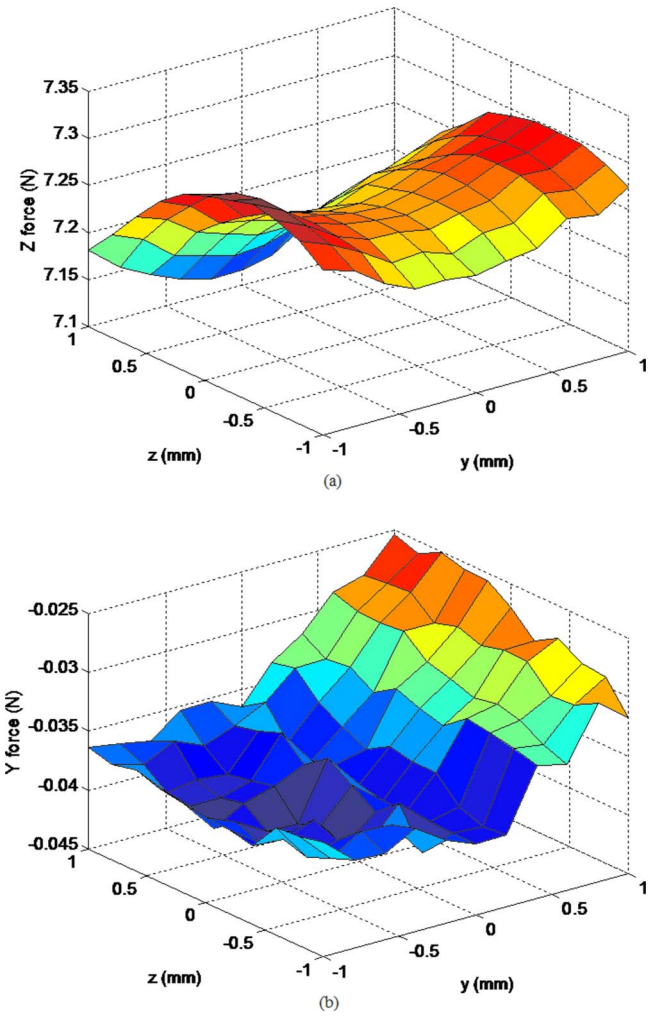

FIG. 16. (Color online) Dynamic force distribution of the prototype: (a) *Z* force, and (b) *Y* force. Color is proportional to the height of surface in each figure (red high, blue low) and note that color scales are not identical in the figures. The nominal dynamic *Z* force is 7.24 N, which is larger than the designed value because of the corner effect of the coil windings. The variation and the shape are almost same as the simulation.

forces can be compensated for by the state observer when a closed-loop control is applied. Next, dynamic forces are measured in the same manner as previously described. A current of 1 A is applied to the stator coil. Figure 16 presents the measured dynamic forces. The nominal dynamic *Z* force is 7.24 N, which is larger than the designed value because of the corner effect of the coil windings. The variation and the shape are almost the same as the simulation.

VI. CONCLUSION

In this paper, we proposed a new HLAMB for a magnetic levitation stage. The HLAMB consists of two Halbach magnet arrays, a target magnet, and two Lorentz coils. Because the Halbach magnet array confines magnetic flux to the target magnet, the HLAMB can have a large static force. Compared to a conventional bearing, the HLAMB achieved a more than fourfold increase in static force. Also, the two symmetric coils embedded between two Halbach magnet arrays create a dynamic force in the same direction as the static force. Therefore, the HLAMB can control its position while simultaneously compensating for load gravity. Through design optimization, large dynamic force, zero stiffness, a small parasitic force, and compact size were guaranteed. The linear characteristic of the dynamic force and zero stiffness eliminates the necessity for nonlinear control such as feedback linearization, which increases the complexity of a controller. In particular, zero stiffness and a small parasitic force can be good advantages when applied to vibration isolation. Therefore, the HLAMB will be widely utilized for high-precision stages and/or active vibration isolation equipment.

[1] A. T. A. Peijnenburg, J. P. M. Vermeulen, and J. Van Eijk, Microelectron. Eng. **83**, 1372 (2006).
[2] D. L. Trumper, W.-J. Kim, and M. E. Williams, IEEE Trans. Ind. Appl. **32**, 371 (1996).
[3] W.-J. Kim and D. L. Trumper, Precis. Eng. **22**, 66 (1998).
[4] M. Williams, P. Faill, P. Bischoff, S. Tracy, and B. Arling, Proc. SPIE **3051**, 856 (1997).
[5] N. Korenaga, U.S. Patent No. 6,873,404 (2005).
[6] M. Binnard, K. Ono, and J. Hazelton, U.S. Patent No. 6,750,625 (2004).
[7] D. Trumper, U.S. Patent No. 5,294,854 (1994).
[8] K.-B. Choi, Y. G. Cho, T. Shinshi, and A. Shimokohbe, Mechatronics **13**, 587 (2003).
[9] G. J. P. Nijsse and J. W. Spronck, U.S. Patent No. 6,402,118 (2002).
[10] S. A. J. Hol, E. Lomonova, and A. J. A. Vandenput, Precis. Eng. **30**, 265 (2006).
[11] K. Halbach, Nucl. Instrum. Methods **169**, 1 (1980).
[12] X. -F. Gou, Y. Yang, and X. -J. Zheng Appl. Math. Mech. **25**, 297 (2004).
[13] F. C. Moon, *Magneto-Solid Mechanics* (Wiley, New York, 1984), pp. 42–44.
[14] P. Venkataraman, *Applied Optimization with MATLAB Programming* (Wiley, New York, 2001), pp. 289–296.
[15] J. S. Arora, *Introduction to Optimum Design* (McGraw-Hill, New York, 1989), pp. 347–425.
[16] C. G. E. Boender and A. H. G. Rinnoy Kan, Math. Program. **37**, 59 (1987).